# Uplink Array Calibration via Power Spectra in the Presence of Phase and Delay Errors

**Victor A. Vilnrotter***

ABSTRACT. — In uplink array operations, alignment of the carrier phase and modulation delay from each antenna is of fundamental importance in achieving maximum array gain. The power spectrum of the combined signal can be obtained at the spacecraft and relayed to the ground for processing, or in near-Earth radar applications the echo signals from small targets can be collected and processed at the ground receiver. Expressions are derived for the power spectrum of a transmitting array of $K$ elements in the presence of phase and delay alignment errors, and simulation results are provided to validate the theoretical results. It is shown that the power spectra are generally sensitive to errors in carrier and modulation alignment, thus enabling uplink array calibration directly from the power spectrum of the combined array signal.

## I. Introduction

The impact of random errors on the combined power of uplink array signals at the spacecraft has been derived in a previous paper [1], and shown to result in an ideal array power gain of $K^2$ over a single antenna for an array of $K$ elements when equal power transmitters are employed, and when both carrier and modulation are perfectly aligned at the spacecraft. Time-varying range due to changing geometry is typically the largest component of signal delay and phase variations, although ground system signal distribution and instrumental delays must also be taken into account. An example of uplink array geometry for a two-element array is shown in Figure 1, illustrating the time-varying range from each antenna to the spacecraft, as Earth rotates and the spacecraft travels along its orbital trajectory. Carrier phase and modulation delay due to geometry are estimated via predicts [2] in order to compensate the transmitted signals; however, even the best predicts are subject to error. Small residual delay ($\Delta$) and phase ($\theta$) errors due to predict and equipment inaccuracies, thermal instabilities, and tropospheric variations lead to losses in combined signal power at the spacecraft and also impact the shape of the received power spectrum. Residual errors in carrier phase and modulation delay can lead to significant degradation in combined power and signal fidelity, which ultimately limits the data throughput at the spacecraft.

* Communications Architectures and Research Section.
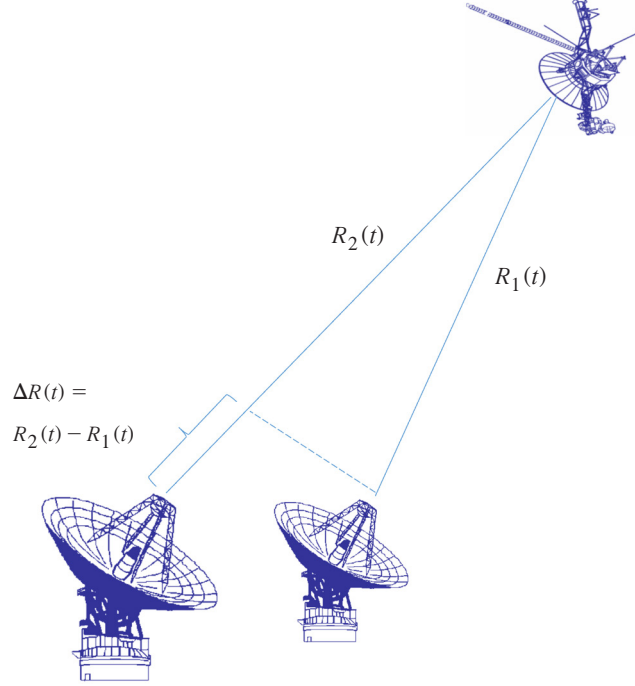
**Figure 1. Two-element uplink array geometry, defining the pathlength to the spacecraft at a particular time $t$, $R_1(t)$ and $R_2(t)$, and pathlength difference $\Delta R(t)$.**

The power spectrum of the combined uplink array signal at the spacecraft, illuminated by an uplink array of $K$ antennas with identical transmitter powers, perfect antenna pointing, and error-free Doppler predicts to remove differential Doppler, depends on the degree of carrier phase and modulation delay alignment that can be achieved on the ground. This is referred to as phase and delay calibration, which must be carried out before any successful uplink array track can take place.

This article addresses the specific problem of uplink array calibration in the presence of carrier phase and phase-modulated pseudo-noise (PN) code delay alignment, assuming that other important operational tasks such as calibration of transmitter powers and predict-driven antenna pointing have been addressed.

## II. Power Spectrum of Uplink Array Signals: Theory

### A. Unmodulated Carrier

It is convenient to represent the signal received at the spacecraft as the real part of the complex signal, $s(t) = \mathrm{Re}\left\{\sqrt{2P}\,\tilde{s}_0(t)e^{j\omega t}\right\}$, where $\tilde{s}_0(t) = d(t)e^{j\theta}$, $d(t) = \pm 1$, $\omega$ is the carrier radian frequency, and define average power as

$$s^2(t) = \left(\mathrm{Re}\left\{\sqrt{2P}\,\tilde{s}_0(t)e^{j\omega t}\right\}\right)^2 = 2Pd^2(t)\left(\mathrm{Re}\left\{e^{j(\omega t+\theta)}\right\}\right)^2 = 2P\cos^2(\omega t+\theta)$$
$$= 2P\left\{\tfrac{1}{2}\left[1+\cos(2\omega t+2\theta)\right]\right\}_{LP} = P.$$

Alternately, we can define average power as the squared magnitude of the complex signal, yielding the same result:

$$s^2(t) = \left| \sqrt{P}\, \tilde{s}_0(t)\, e^{j\omega t} \right|^2 = P\!\left( d^2(t)\, e^{j\omega t} e^{-j\omega t} \right) = P. \tag{1}$$

Clearly, the mathematical description is much simpler when the complex model is employed; therefore, we adopt the complex signal representation in the rest of this article.

Consider an uplink array of $K$ elements, each radiating an unmodulated Doppler-compensated carrier with random residual phase specified by the phase vector $\boldsymbol{\theta} = (\theta_1, \theta_2, \cdots, \theta_i, \cdots, \theta_K)$. Each received complex signal at the spacecraft can be described in terms of a phasor diagram, as shown in Figure 2.
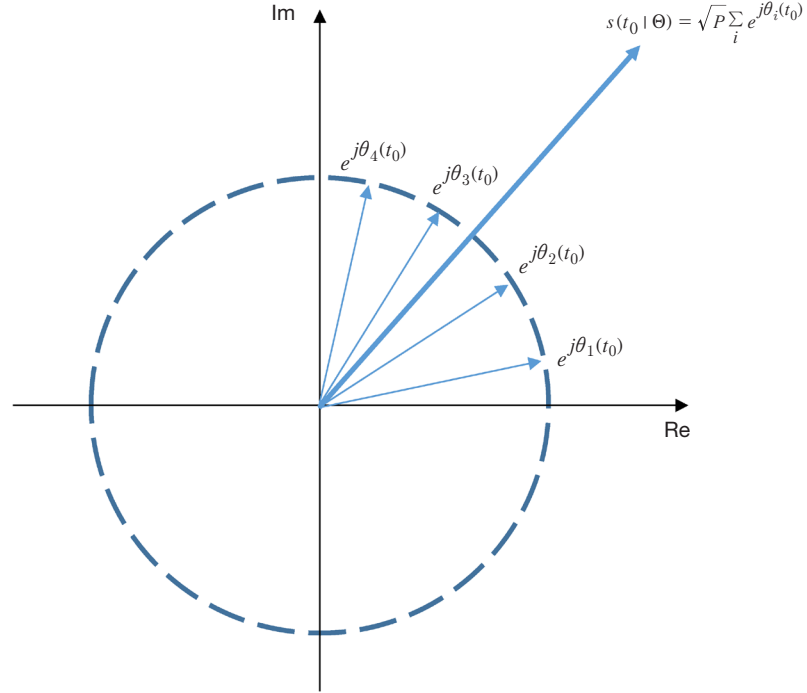


**Figure 2. Phasor diagram of individual signals and sum of uplink array signals at the spacecraft, for a specific realization of a 4-dimensional array phase vector.**

We shall make the realistic assumption that each component of the phase vector changes slowly enough so that the phase can be assumed constant over a suitably small time interval, for purposes of analysis. With this model, Figure 2 describes the phase vector at a particular time $t_0$, which may evolve with time to a different realization of the phase vector at a later time. At any given time $t$, the combined signal can be represented as the sum of the complex envelopes, $s(t|\boldsymbol{\theta}) = \sqrt{P}\sum_i e^{j\theta_i(t)}$, where each array element transmits $P$ watts of power. The combined power at the spacecraft can be expressed as the squared magnitude of the complex envelopes, as shown in [1]:

$$|s(t|\boldsymbol{\theta})|^2 = \left| \sqrt{P} \sum_{i=1}^{K} e^{j\theta_i(t)} \right|^2 = P\left( \sum_{i=1}^{K} \sum_{k=1}^{K} e^{j[\theta_i(t) - \theta_k(t)]} \right)$$

$$= P\left( \sum_{i=1}^{K} e^{j[\theta_i(t) - \theta_i(t)]} + \sum_{i=1}^{K} \sum_{\substack{k=1 \\ k \neq i}}^{K} e^{j[\theta_i(t) - \theta_k(t)]} \right) = P\left( K + \sum_{i=1}^{K} \sum_{\substack{k=1 \\ k \neq i}}^{K} e^{j[\theta_i(t) - \theta_k(t)]} \right). \tag{2}$$

The phase component $\theta_i(t)$ represents the time-evolution of the residual carrier phase from the $i$-th antenna, after the known component of phase variation due to Doppler has been removed via predicts [2], and after propagating through the atmosphere added a random component due to variations in refractive index that induce different propagation delays. During the time interval corresponding to a track, the random residual phase function can often be characterized adequately by its second-order statistics, namely a mean value $\overline{\theta}_i$ and a zero-mean fluctuation about this mean value defined by the variance $\sigma_{\theta_i}^2$. If these statistics can be assumed constant over a short observation time $T$, then the time variable $t$ can be dropped from $\theta_i(t)$ to simplify notation, yielding $\theta_i$. This approximation enables the representation of the phase error with a vector of phase errors $\boldsymbol{\theta} = (\theta_1, \theta_2, \cdots, \theta_i, \cdots, \theta_K)$, where each component is a slowly varying random variable that is assumed to be constant over the observation interval.

A general solution for the average uplink array power at the spacecraft has been obtained in [1], assuming Gaussian statistics for the phase error. This model is valid when the variance of the phase errors is small compared to a radian, hence virtually all of the probability density is contained within the range $-\pi < \theta_i \leq \pi$ for all $i$, over the time interval $0 < t \leq \mathcal{T}$. Using the joint probability density for a Gaussian random vector $\boldsymbol{\theta} = (\theta_1, \theta_2, \cdots, \theta_K)$ with arbitrary mean values, variances, and pairwise correlations, given by the following expression:

$$p(\boldsymbol{\theta}) = \frac{\exp\left[ -\frac{1}{2}(\boldsymbol{\theta} - \overline{\boldsymbol{\theta}})\Lambda_\theta^{-1}(\boldsymbol{\theta} - \overline{\boldsymbol{\theta}})^T \right]}{(2\pi)^{K/2} |\Lambda_\theta|^{1/2}}, \tag{3}$$

where $\overline{\boldsymbol{\theta}} = (\overline{\theta}_1, \overline{\theta}_2 \cdots, \overline{\theta}_K)$, $\Lambda_\theta = E\{(\boldsymbol{\theta} - \overline{\boldsymbol{\theta}})^T(\boldsymbol{\theta} - \overline{\boldsymbol{\theta}})\}$, $\sigma_{\theta_i}^2 = E(\theta_i - \overline{\theta}_i)^2$, and $\lambda_{\theta_{i,k}} = E\{(\theta_i - \overline{\theta}_i)(\theta_k - \overline{\theta}_k)\}$, the following expression was obtained for the average power of the combined uplink array carriers over the interval $0 < t \leq \mathcal{T}$, averaged over the statistics of the phase error vector:

$$\overline{|s(t|\boldsymbol{\theta})|^2}^\theta = P\left( K + 2 \sum_{i=1}^{K-1} \sum_{k>i}^{K} \exp\left[ -\frac{1}{2}\left( \sigma_{\theta_i}^2 + \sigma_{\theta_k}^2 - 2\lambda_{\theta_{i,k}} \right) \right] \cos\left( \overline{\theta}_i - \overline{\theta}_k \right) \right). \tag{4}$$

It is interesting to examine the limiting case where the variance of the phase error is negligibly small compared to its mean value over the observation interval, and hence can be approximated by zero: $\sigma_{\theta_i}^2 << \overline{\theta}_i \cong 0$. This corresponds to the deterministic case with nonrandom but unknown phase errors characterized by the mean-value vector $\overline{\boldsymbol{\theta}} = (\overline{\theta}_1, \overline{\theta}_2, \cdots, \overline{\theta}_K)$. In this case, Equation (4) reduces to the following expression:

$$\overline{|s(t|\boldsymbol{\theta})|^2}^\theta = P\left( K + 2 \sum_{i=1}^{K-1} \sum_{k>i}^{K} \cos\left( \overline{\theta}_i - \overline{\theta}_k \right) \right), \tag{5}$$

which depends on all pairwise differences of mean phase errors. This is the case of greatest interest in this article, corresponding to a short observation interval where the phase errors can be approximated by nonrandom but unknown constants, which can be estimated from a vector of samples of the received signal waveform obtained at the spacecraft and relayed to the ground. Equivalently, the vector of samples could be obtained from a ground receiver observing radar echoes from a nearby target such as a near-Earth asteroid.

Note that if the phase error components are all equal, the double sum in Equation (5) reduces to

$$2 \sum_{i=1}^{K-1} \sum_{k>i}^{K} \cos(\overline{\theta}_i - \overline{\theta}_k) \bigg|_{\overline{\theta}_i = \overline{\theta}_k} = K(K-1), \qquad (6)$$

yielding the following combined power at the spacecraft:

$$\overline{|s(t|\boldsymbol{\theta})|^2}^{\theta} \bigg|_{\overline{\theta}_i = \overline{\theta}_k} P\left(K + 2 \sum_{i=1}^{K-1} \sum_{k>i}^{K} \cos(\overline{\theta}_i - \overline{\theta}_k)\right) = P(K + K(K-1)) = PK^2, \qquad (7)$$

which is seen to correspond to the maximum power possible with an ideally coherent uplink array of $K$ antennas, all with the same transmitter power. This result confirms the heuristic notion that the phase errors need not be zero for ideal uplink array performance: it is sufficient that the phase errors are all the same.

### B. Phase-Modulated Carrier

A phase-modulated residual-carrier signal can be represented as an electromagnetic wave of the form

$$s(t) = \text{Re}\left\{A \exp\left[j(\omega t + \varphi_r \varphi(t))\right]\right\} = A \cos\left[j(\omega t + \varphi_r \varphi(t))\right] \qquad (8)$$

where $\varphi(t) = \sum_{i=-\infty}^{\infty} d_i p(t - iT)$ is the data or PN code waveform consisting of a sequence of $T$ second pulses, $\varphi_r$ is the modulation index in radians, $d_i = \pm 1$ is binary modulation corresponding to random (0,1) data or to a binary PN sequence, $p(t)$ is a pulse-shape defined over the symbol interval $(0, T]$. If stable coherent addition of the uplink array signals is to be achieved, there can be no error in the uplink frequencies, hence we can ignore the frequency term in Equation (8) and focus entirely on the residual carrier phase and modulation delays as the only sources of error in the uplink array application. In practice, this is achieved by the use of highly accurate frequency predicts, as described in [2].

We define a hypothetical normalized reference signal as $\tilde{s}_0(t) = \exp[j\varphi_r \varphi(t)]$, and further define the $k$-th transmitted signal referenced to $\tilde{s}_0(t)$ as $\tilde{s}_k(t) = A_k \exp[j(\varphi_r \varphi(t - \Delta_k) + \theta_k)]$, where $A_k$ denotes the amplitude of the $k$-th signal, containing both a residual delay $\Delta_k$ and a residual phase $\theta_k$.

For an uplink array consisting of $K$ antennas, the combined signal can be expressed as the sum of the complex components:

$$\tilde{s}(t) \sum_{k=1}^{K} A_k \exp\left[j\left(\varphi_r \varphi(t - \Delta_k) + \theta_k\right)\right].$$

The residual phase and delay of the array can now be specified by the vectors $\Delta = (\Delta_1, \Delta_2, \ldots, \Delta_K)$ and $\Theta = (\theta_1, \theta_2, \ldots, \theta_K)$, hence the combined signal at the target, conditioned on the residual delay and phase error vectors $\Delta$ and $\Theta$, can be expressed as

$$\tilde{s}(t \,|\, \Delta, \Theta) = \sum_k A_k \exp(j\theta_k) \tilde{s}_0(t - \Delta_k). \tag{9}$$

Denoting the Fourier transform of the combined signal as $\tilde{S}(f \,|\, \Delta, \Theta) \equiv \mathcal{F}\{\tilde{s}(t \,|\, \Delta, \Theta)\}$, and recalling that delay in the time domain by $\Delta_k$ seconds corresponds to multiplication by $\exp[-j2\pi f \Delta_k]$ in the frequency domain, the Fourier transform of the combined signal in Equation (9) can be expressed as

$$\tilde{S}(f \,|\, \Delta, \Theta) = \sum_{k=1}^{K} A_k \exp(j\theta_k) \mathcal{F}\{\tilde{s}_0(t) \exp(-j2\pi f \Delta_k)\} = \tilde{S}_0(f) \sum_{k=1}^{K} A_k \exp[j(-2\pi f \Delta_k + \theta_k)]. \tag{10}$$

Note that the Fourier transform of the combined signal with residual delays and phases yields an expression consisting of the Fourier transform of the reference signal, $\tilde{S}_0(f)$, multiplied by a sum that depends only on the residual delays and phases, interpreted here as the channel transfer function (CTF) of the uplink array channel:

$$H_K(f \,|\, \Delta, \Theta) \equiv \sum_{k=1}^{K} A_k \exp[j(-2\pi f \Delta_k + \theta_k)]. \tag{11}$$

Hence, using Equation (10), Equation (9) can be expressed in more compact form as

$$\tilde{S}(f \,|\, \Delta, \Theta) = \tilde{S}_0(f) H_K(f \,|\, \Delta, \Theta). \tag{12}$$

Taking the squared magnitude of Equation (12) yields the following expression as the kernel of the power spectrum estimate: $\left|\tilde{S}(f \,|\, \Delta, \Theta)\right|^2 = \left|\tilde{S}_0(f)\right|^2 \left|H_K(f \,|\, \Delta, \Theta)\right|^2$.

The Fourier transform of the generic reference signal can often be derived analytically from the structure of the time function. For example, random NRZ data consisting of $T$ second rectangular pulses, or PN sequences that resemble random NRZ data, yield a power spectrum of the form $\left|\tilde{S}_0(f)\right|^2 = \sin^2(\pi f T)/(\pi f T)^2$. The squared magnitude of the CTF can be evaluated as follows:

$$\begin{aligned} \left|H_K(f \,|\, \Delta, \Theta)\right|^2 &\equiv \left|\sum_{k=1}^{K} A_k \exp[j(-2\pi f \Delta_k + \theta_k)]\right|^2 \\ &= \left(\sum_{k=1}^{K} A_k \exp[j(-2\pi f \Delta_k + \theta_k)]\right)\left(\sum_{m=1}^{K} A_m \exp[-j(-2\pi f \Delta_m + \theta_m)]\right) \\ &= \sum_{k=1}^{K} A_k^2 + \sum_{\substack{k \\ k \neq m}} \sum_{m} A_k A_m \exp\{j[-2\pi f(\Delta_k - \Delta_m) + (\theta_k - \theta_m)]\}. \end{aligned} \tag{13}$$

The expression in Equation (13) can be further reduced using the following operations:

$$\sum_{\substack{k \\ k \neq m}} \sum_m A_k A_m \exp\left[j\left(-2\pi f(\Delta_k - \Delta_m) + (\theta_k - \theta_m)\right)\right]$$

$$= \sum_{m=1}^{K-1} \sum_{k>m}^{K} A_k A_m \exp\left[j\left(-2\pi f(\Delta_k - \Delta_m) + (\theta_k - \theta_m)\right)\right] + \sum_{k=1}^{K-1} \sum_{m>k}^{K} A_k A_m \exp\left[j\left(-2\pi f(\Delta_k - \Delta_m) + (\theta_k - \theta_m)\right)\right]$$

$$= \sum_{m=1}^{K-1} \left[ \sum_{k>m}^{K} A_k A_m \exp\left[j\left(-2\pi f(\Delta_k - \Delta_m) + (\theta_k - \theta_m)\right)\right] + \sum_{k>m}^{K} A_k A_m \exp\left[-j\left(-2\pi f(\Delta_k - \Delta_m) + (\theta_k - \theta_m)\right)\right] \right]$$

$$= 2 \sum_{m=1}^{K-1} \left[ \sum_{k>m}^{K} A_k A_m \cos\left[-2\pi f(\Delta_k - \Delta_m) + (\theta_k - \theta_m)\right] \right]. \tag{14}$$

The last equality in Equation (14) follows from the fact that there are an equal number of complex exponential terms with argument $(\Delta_k - \Delta_m)$ and $(\Delta_m - \Delta_k) = -(\Delta_k - \Delta_m)$, and similarly for $(\theta_k - \theta_m)$; hence, combining these terms pairwise yields the sum of the cosine terms in the last equality of Equation (14). Substituting into Equation (13) yields the following simplified form of the squared magnitude of the CTF:

$$\left| H_K(f | \Delta, \Theta) \right|^2 = \sum_{k=1}^{K} A_k^2 + 2 \sum_{m=1}^{K-1} \left[ \sum_{k>m}^{K} A_k A_m \cos\left[-2\pi f(\Delta_k - \Delta_m) + (\theta_k - \theta_m)\right] \right]. \tag{15}$$

Note that $(\Delta_k - \Delta_m)$ and $(\theta_k - \theta_m)$ are the differential delays and phases, respectively, associated with each baseline. There are a total of $K(K-1)/2$ terms in the double-sum, implying that every baseline contributes to the CTF and hence implies that this many measurements would be needed to completely characterize the CTF. However, we further note that each baseline delay and phase can be referred to a "reference" antenna, designated by the subscript "1," by rewriting each term as $(\Delta_k - \Delta_m) = (\Delta_k - \Delta_1) - (\Delta_m - \Delta_1)$. In other words, each baseline term in Equation (15) can be expressed as the difference of baseline terms measured from a single reference antenna, henceforth termed the "reference baseline." Since there are $(K-1)$ reference baselines, and recalling that for $K > 2$ it is always true that $K(K-1)/2 \underset{K>2}{>} K-1$, this implies that the number of measurements required to characterize the CTF can be significantly reduced for the case of a large array, where $K \gg 2$. To illustrate this point, note that for $K = 2, K(K-1)/2 = (K-1) = 1$, hence both terms are equal to 1; but for $K = 16, K(K-1)/2 = 120$ differential-baseline measurements would be required, whereas only $(K-1) = 15$ reference-baseline measurements are needed, together with simple calculations to form the differences, to characterize the CTF. However, this approach applies only to perfect measurements of the reference-baseline, implying negligible noise or equivalently very high signal-to-noise ratio. In the presence of significant additive noise in the data, additional baseline measurements will tend to reduce the error in the measured CTF, resulting in better uplink array performance, but the theoretical development of the mathematical model incorporating additive noise is beyond the scope of this article.

As an example of the application of Equation (15), the CTF for a two-element array is

$$\left| H_2(f | \Delta, \Theta) \right|^2 = \left( A_1^2 + A_2^2 \right) + 2 A_1 A_2 \cos\left[-2\pi f(\Delta_1 - \Delta_2) + (\theta_1 - \theta_2)\right], \tag{16}$$

while for a three-element array, the CTF becomes

$$\left|H_3\left(f|\mathbf{\Delta},\Theta\right)\right|^2 = \left(A_1^2 + A_2^2 + A_3^2\right) + 2\Big\{A_1A_2\cos\left[-2\pi f(\Delta_1 - \Delta_2) + (\theta_1 - \theta_2)\right]$$
$$+ A_1A_3\cos\left[-2\pi f(\Delta_1 - \Delta_3) + (\theta_1 - \theta_3)\right] + A_2A_3\cos\left[-2\pi f(\Delta_2 - \Delta_3) + (\theta_2 - \theta_3)\right].$$

(17)

Examples of a three-element CTF and the corresponding computed power spectrum for a PN-11 modulated signal are shown in Figures 3(a) and 3(b), with delay and phase vectors (0.25, 0.5, 1) chips and (–1, pi/2, 0.7) radians, respectively, together with the known expression for the power spectrum of random binary data: $\left|\tilde{S}_0(f)\right|^2 = \sin^2(\pi fT)/(\pi fT)^2$. Note that the CTFs are always periodic functions of frequency, as expected for the sum of cosine terms in Equations (16) and (17).
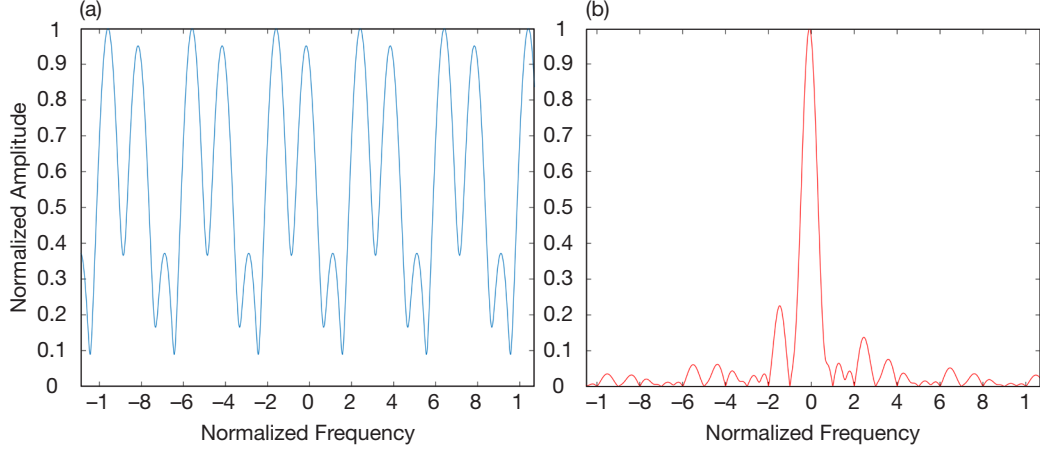


Figure 3. (a) Calculated normalized CTF of three-element uplink array channel; (b) calculated normalized power spectrum of PN-11 modulated signal, corresponding to the CTF.

## III. Simulated Power Spectra of PN-Modulated Uplink Array Signals

A MATLAB program has been developed to simulate the complex envelopes of uplink array signals phase-modulated by PN codes, and determine their power spectra for any combination of array and signal parameters, in order to validate the theoretical results. The current version of the program simulates signals and power spectra for two- and three-element uplink arrays, but can be extended to larger arrays due to an inherently modular construction. It generates NRZ PN-11 sequences by specifying $d_i$ in the phase-modulation function

$$\varphi(t) = \sum_{i=\infty}^{\infty} d_i p(t - iT).$$

The examples shown in Figures 4(a), (b), and (c) illustrate the behavior of two- and three-element uplink array spectra on a linear scale, normalized to the pulse duration $T$, with zero delay and phase errors, and also with arbitrary delay and phase errors applied to the uplink signals. Note that with zero phase and delay errors, the power spectra of two- and three-element arrays shown in Figure 4(a) are simply scaled versions of the well-known random data spectrum $\left|\tilde{S}_0(f)\right|^2 = \sin^2(\pi fT)/(\pi fT)^2$. Note the close agreement between theory and simulation, even in the minutest details, confirming the validity of the theoretical results, on which the estimation techniques are based.
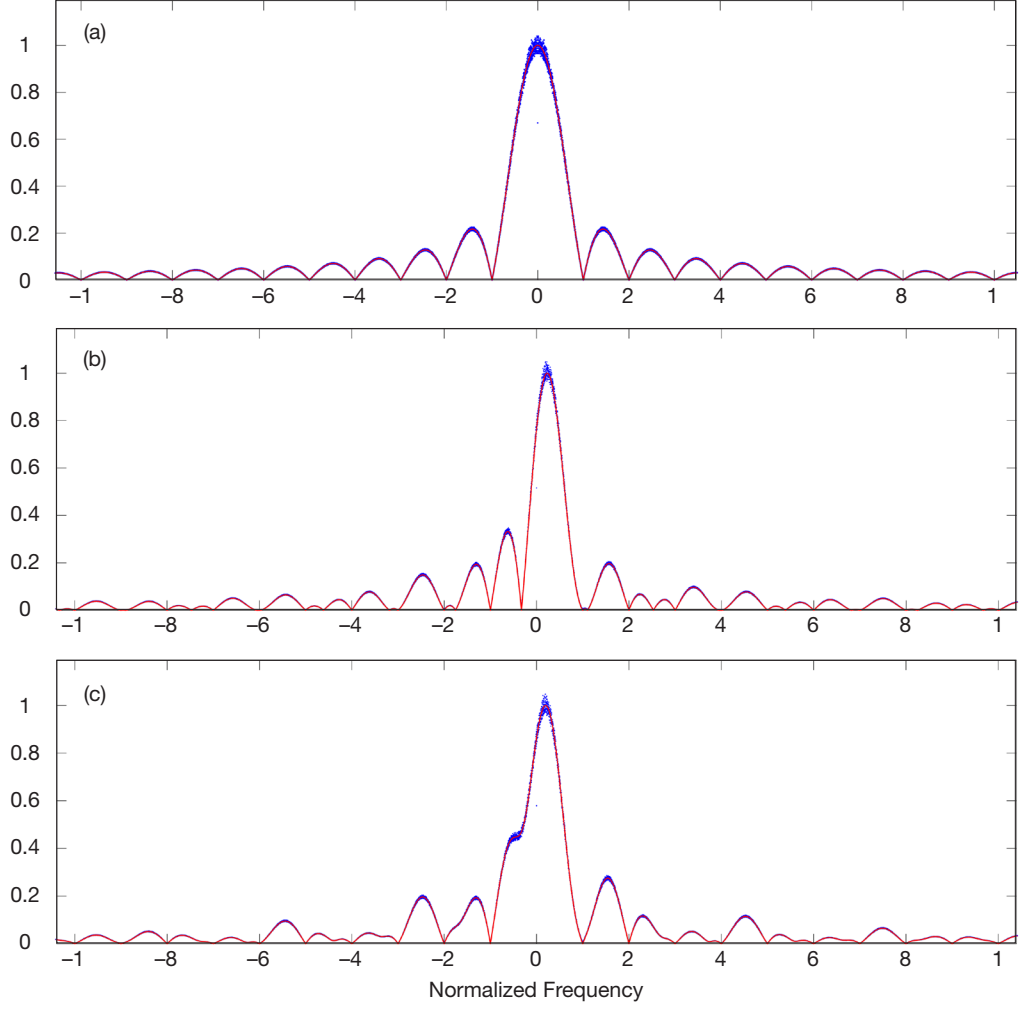
Figure 4. Comparison of computed and simulated normalized power spectra for a two-element and three-element uplink arrays, on a linear scale: (a) zero phase and delay errors, valid for two- and three-element arrays; (b) two-element array, with arbitrary phase and delay errors; (c) three-element array, with arbitrary phase and delay errors. Simulation: blue dots, theory: red lines.

With both phase and delay errors present, it is clear from Figures 4(b) and 4(c) that the continuous spectra obtained from complex baseband samples are asymmetric for both two- and three-element uplink arrays, as suggested previously in Figure 3(b). However, the continuous spectra of Figures 5(a) and (b) show that when the phase errors are set to zero, and hence only delay errors are present, the power spectra become fully symmetric for both two- and three-element uplink arrays.

Therefore, examination of the recorded spectra for symmetry reveals the presence or absence of significant phase errors. The phase errors could be estimated simultaneously with the delay errors by searching over a $(K-1) \times (K-1)$ dimensional delay-phase parameter space, however this approach is computationally intensive for large arrays. A simpler approach is to estimate the phase errors relative to a reference antenna via phase-ramps, using techniques developed previously for carrier phase alignment and reported in [3,4].
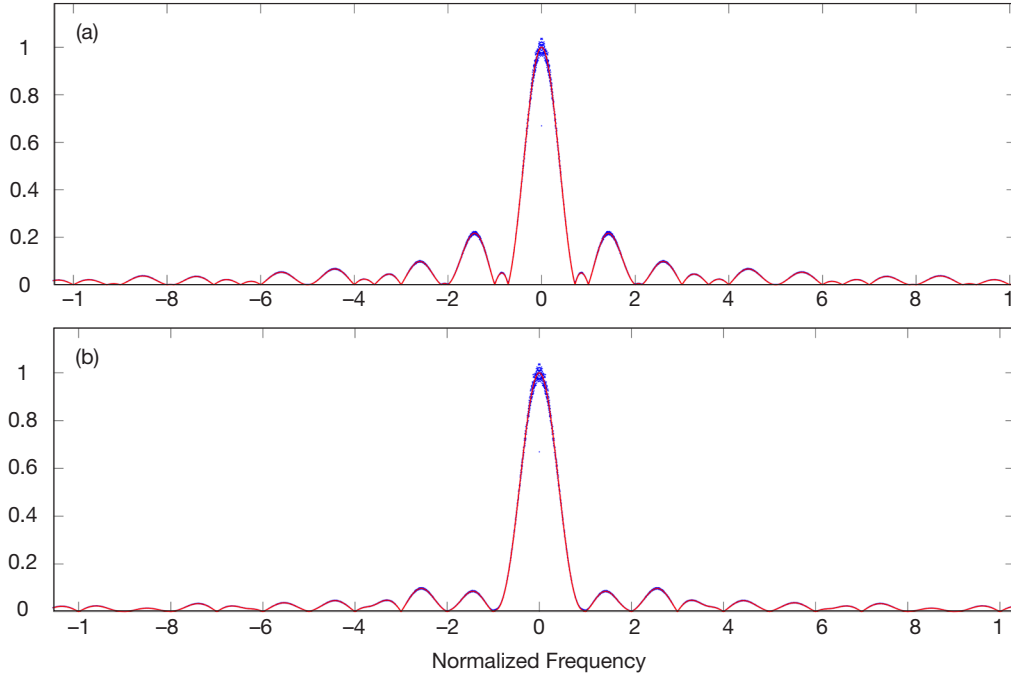
**Figure 5. Normalized power spectra with zero phase but arbitrary delay errors:
(a) two-element uplink array; (b) three-element uplink array.**

We adopt this latter approach here, and concentrate on the problem of estimating modulation delay, after the carrier phase has been estimated and compensated in the uplink array signals.

## IV. Estimation of Uplink Array Delay Errors from Recorded Power Spectra

The theory and simulation described above can be applied to the problem of estimating the parameters of the uplink array signals, derived directly from the recorded spectra. The parameter of greatest interest here is modulation delay; however, other relevant signal parameters such as modulation index, signal amplitude or power, and phase-modulator filter bandwidth can also be estimated for the observed power spectra [5]. The estimation of multiple signal parameters from recorded spectra implies search over a multidimensional parameter space, which may be computationally intensive especially if the uncertainty range is large.

One way to mitigate the problem of parameter search over a multidimensional space is to reduce the size of the uncertainty region, by preparing templates of rough-quantized parameters to bracket the observed spectra. For example, if we make the reasonable assumption that transmitter calibration and antenna pointing are accurate, so that we can set the signal amplitudes equal at the target, and in addition assume that delay error does not exceed one chip, then only fractional-chip delay and phase remain to be estimated. An example of simulated spectra in dB, rough quantized to quarter-chip delays and $\pi/2$ phase is shown in Figure 6, where the modulation index and filter bandwidth have been set to arbitrary values. Four such templates have been generated for all four quarter-chip delays, but only the 1/4 chip delay is shown in Figure 6.
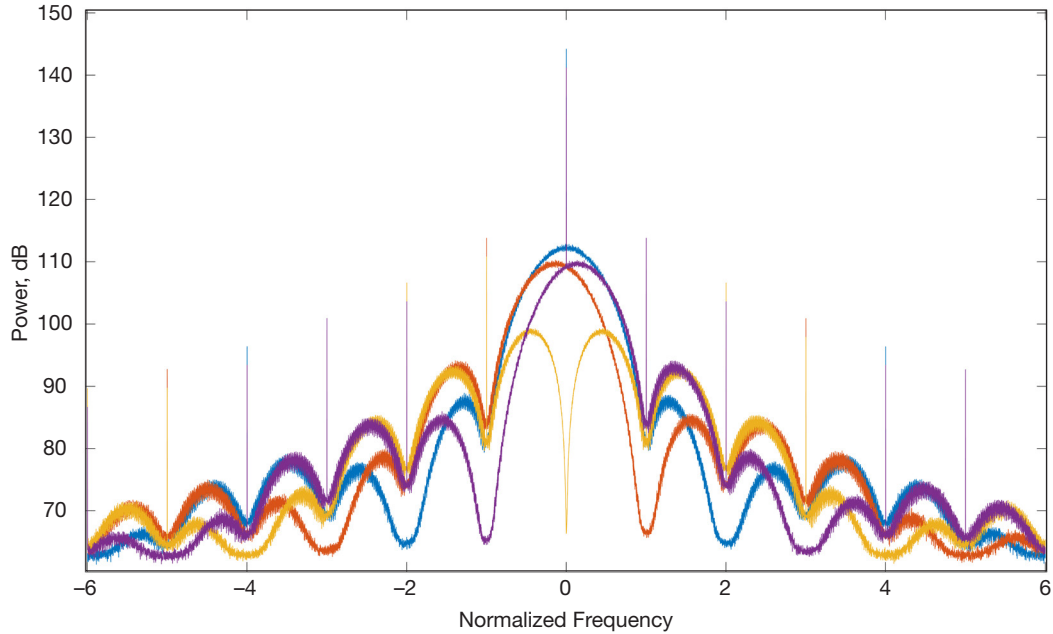
**Figure 6. Simulated power spectra of signals phase modulated with filtered PN-11 code with residual carrier, with delay set to 1/4 chip, and phase quantized to $\pi/2$ radians.**

Given an observed spectrum, it can be compared to predetermined templates of the kind shown in Figure 6, and the "best match" to the rough-quantized delay and phase determined. Using this as a starting point, the dimensions of the uncertainty region can be computed, and algorithms designed to refine the estimates to the required accuracy can be applied.

For example, the modulation index can be estimated directly from the observed spectra by measuring the difference between the peak of the residual carrier and the modulation at the same frequency in dB, representing carrier suppression. Using the undistorted zero-error blue curve in Figure 6, it can be seen that the peak of the residual carrier is at 145 dBm, whereas the continuous modulated spectrum at the same frequency is approximately 112 dBm, hence the carrier suppression is 145 –112 = 33 dB. It should be noted that the same value of carrier suppression would be obtained from any of the distorted curves in Figure 6, such as the purple curve representing 1/4 chip delay and $\pi/2$ radians phase error, hence the estimation of the modulation index is relatively straightforward as long as good quality recordings of the spectra are available. Note that carrier suppression impacts the relative powers in the residual carrier and the modulation, but does not affect the shape of the continuous spectrum.

The discrete components at the nulls of the continuous spectra are caused by filtering of the modulating waveform before applying it to the phase modulator, as explained in [5]. With unfiltered waveforms and infinite bandwidth modulators the discrete components disappear; however, some degree of filtering is always present in real systems. The most relevant parameter here is the effective bandwidth of the modulator or of the filter preceding the modulator, which can be estimated from the strength of the discrete components

occurring at the nulls, using predetermined spectra similar to Figure 6, but indexed in modulator bandwidth. For this simulation a first-order Butterworth filter was used, with a bandwidth corresponding to 90 percent of the effective modulation bandwidth, to generate the spectra shown in Figure 6. Once the type of filter is determined, the measured strength of the discrete components can be used to estimate the filter bandwidth, similar to the technique used to estimate the modulation index described above. However, a detailed explanation of this approach is beyond the scope of this article. The discrete components at the nulls begin to show up at relatively large filter bandwidths that do not affect the continuous spectrum significantly, especially in the vicinity of the main lobe where spectral estimation takes place in realistic situations. In the following analysis we assume that the phase modulator or filter bandwidth is large enough to fully accommodate the modulation, and hence the discrete components are small enough to be neglected in the following development.

### Estimation of Differential Delay

After carrier phase errors have been corrected using the techniques developed and reported earlier, differential delays between antennas that affect the modulation must be estimated and compensated for best uplink array performance. The approach suggested here is quite general, and can be applied whenever high-quality spectra of the uplink array signals are available, either recorded at the spacecraft and relayed to the ground, or obtained directly on the ground from radar echoes.

The estimation algorithm considered here assumes the availability of a parameterized model of the desired test function (in this case, the power spectrum), which is compared to the observed spectrum, and the parameters corresponding to the best fit to the data are selected. This approach relies on accurate models of the underlying function to be tested, therefore it is paramount to develop an accurate model of the underlying function in terms of the desired parameters, that enable minimization of the mean squared error between the model and the observation with the required resolution. This criterion is illustrated in Figures 7 and 8, which show both simulated and theoretically derived spectra with integer-chip and fractional-chip delays, validating the accuracy of the theoretical model for estimating delay errors.

### Integer-Chip Delays

Power spectra for two-element and three-element arrays with integer (0, 1, 2 chip) delay errors but no phase error, are shown in Figures 7(a) and 7(b). Note that for both two- and three-element arrays, the integer delay can be determined by inspection, simply by counting the number of subpeaks from the peak of the main lobe to the first zero. For example, with a 1-chip delay error, there is exactly one subpeak; for 2-chip delay error, there are two subpeaks; etc.

### Fractional Chip Delays

For fractional delay errors, first the integer part can be approximated by inspection, after which fractional delays can be estimated via the techniques described here. Figures 8(a) and 8(b) illustrate the behavior of the spectra with fractional delay errors corresponding to (0, 0.25, 0.5) chips.
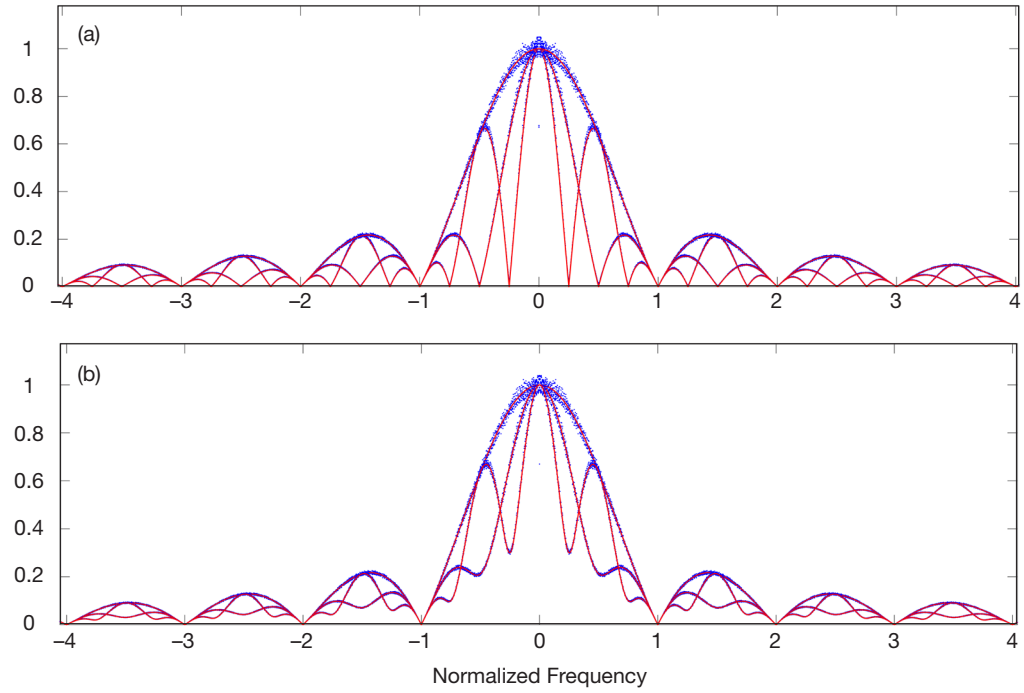
**Figure 7.** Comparison of simulated (blue dots) and theoretically derived normalized power spectrum models, for (a) two-element array with integer chip delays of 0, 1, and 2 chips; and (b) same for a three-element array.
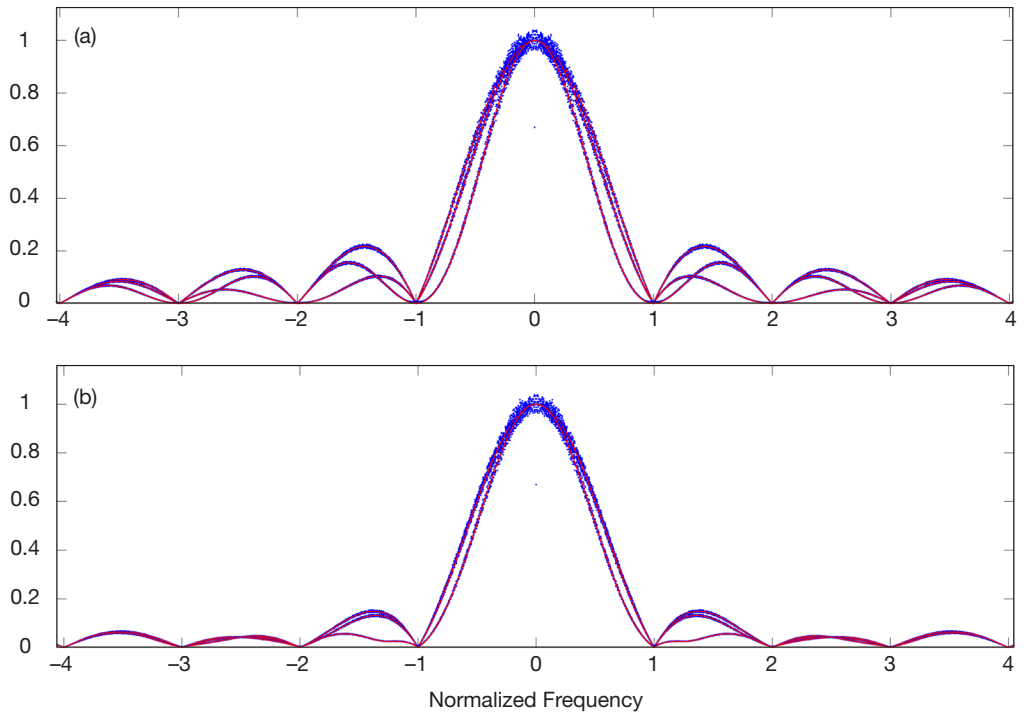


**Figure 8.** Comparison of simulated (blue dots) and theoretically derived (red lines) normalized power spectrum models, for (a) two-element array with fractional chip delays of 0, 0.25, and 0.5 chips; and (b) same for a three-element array, with constant 0.2 chip delay on the third antenna.

These above spectra were obtained from a long waveform of consecutive PN chips, using PN-11 sequences consisting of 2047 chips per sequence with 100 samples per chip. Fast Fourier transforms (FFTs) were computed for vectors of 100,000 samples, then 100 of the FFTs were averaged to reduce the variance of the sample spectra, yielding the simulated spectra shown in the figures, in order to establish a bound on performance. It is evident in Figure 8 that delay errors smaller than 0.25 chips can be resolved visually in the absence of noise.

Delay Estimation Algorithm Structure and Performance

Having demonstrated the accuracy of the theoretical model for the spectra of uplink array signals phase-modulated by random or pseudorandom data in the presence of carrier phase and modulation delay errors, the approach described above can be used to estimate differential delay based on the observed spectra. This technique is illustrated in Figure 9, where a sequence of two-element spectra are shown covering the range of an entire chip delay in 10 equal increments of 0.1 chips. The zero chip delay corresponds to the outermost curve, with the 1 chip delay being innermost. The received spectrum was simulated with a differential delay of 0.67 chips, shown by the blue dots between the 0.6 and 0.7 chip delay curves in Figure 9. It is intuitively clear that the best guess for the delay error in this case corresponds to the theoretical curve closest to the simulated data, or 0.7 chips, in this example.
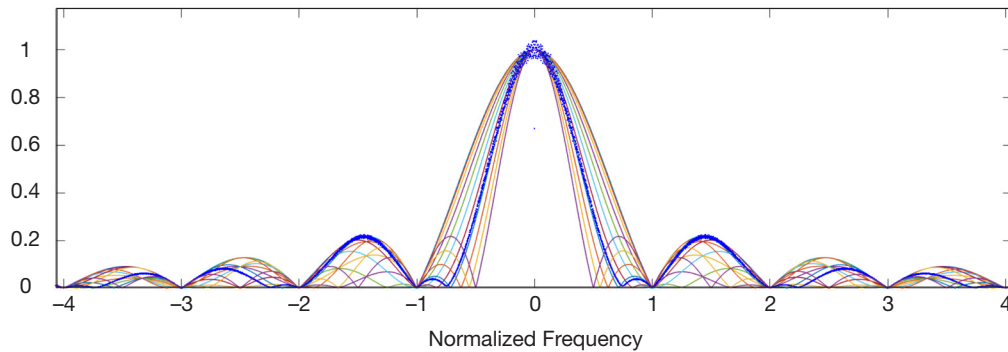


**Figure 9. Sequence of 10 normalized test spectra for a two-element uplink array, computed for 0.1 chip delays covering an uncertainty region of 1 chip, and simulated spectrum corresponding to 0.67 chip delay.**

The delay estimation algorithm is based on the minimum mean-squared error criterion, whereby the delay parameter is varied over the uncertainty range and the parameterized theoretical model computed for a set of values representing the required quantization level. The mean-squared error between the observed data and the theoretical model is computed for the range of parameters of interest, and the parameter yielding the smallest mean-squared error selected.

A plot of the mean-squared error between the simulation and the theoretical model is shown in Figure 10, with model quantization of 0.1 chips, for the simulated spectrum with 0.67 chip delay shown in Figure 9. The mean-squared error curve shows the minimum at 0.7 chips, as expected. It should be noted that if greater accuracy is required, the quantization steps can be decreased, or an interpolation algorithm can be employed to refine the estimates.
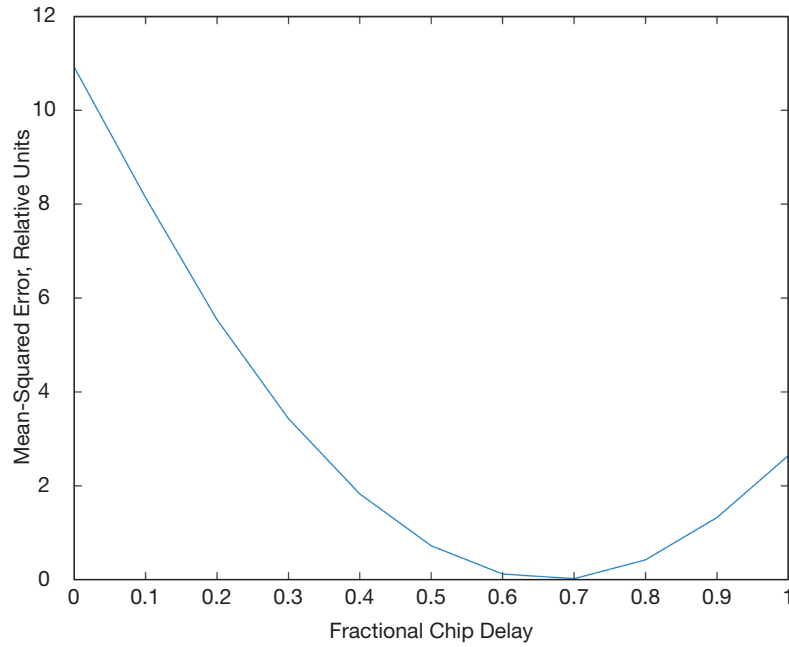
**Figure 10. Minimum mean squared error as a function of fractional delay, for a simulated delay of 0.67 chips.**

## V. Conclusions

The power spectrum has been derived for an arbitrary K-element uplink array, and exact expressions obtained for the spectra in the presence of phase and delay errors. It was shown that uplink array calibration for phase and delay errors can be accomplished with only K-1 measurements, when the signal-to-noise ratio is sufficiently high. Simulation was developed to validate the theoretical results, and close correspondence between theory and simulation established for two and three element arrays. A minimum mean-squared error algorithm was developed to estimate modulation delay for PN coded signals, and the structure and performance of the algorithm demonstrated by example in the high-SNR case, where noise power can be neglected. The incorporation of noise effects on the structure and performance of the delay estimator is beyond the scope of this article, and remains the subject of future research.

## References

[1]  V. Vilnrotter, "Power Spectrum of Uplink Array Signals," *Proceedings of the IEEE Aerospace Conference*, Big Sky, Montana, March 2012.

[2]  P. Tsao, V. Vilnrotter, and V. Jamnejad, "Pointing-Vector and Velocity Based Frequency Predicts for Deep-Space Uplink Array Applications," *Proceedings of the IEEE Aerospace Conference*, Big Sky, Montana, March 2009.

[3]  V. Vilnrotter, D. Lee, P. Tsao, T. Cornish, and L. Paal, "Uplink Array Calibration via Lunar Doppler-Delay Imaging," *Proceedings of the IEEE Aerospace Conference*, Big Sky, Montana, March 2010.

[4]  V. Vilnrotter, D. Lee, T. Cornish, P. Tsao, L. Paal, and V. Jamnejad, "Uplink Array Concept Demonstration with the EPOXI Spacecraft," *Proceedings of the IEEE Aerospace Conference*, Big Sky, Montana, March 2010.

[5]  V. Vilnrotter and D. Lee, "Mitigation of Discrete Spectral Components in Filtered BPSK and OQPSK Signals," *The Interplanetary Network Progress Report*, vol. 42-208, Jet Propulsion Laboratory, Pasadena, California, pp. 1–25, February 15, 2017. http://ipnpr.jpl.nasa.gov/progress_report/42-208/208A.pdf